

Flagella bending affects macroscopic properties of bacterial suspensions

M. Potomkin¹, M. Tournus², L. Berlyand¹, I. S. Aranson^{3,4}

February 8, 2020

¹Pennsylvania State University, Mathematics Department, University Park, Pennsylvania 16802, USA ²Aix Marseille Univ, CNRS, Centrale Marseille, I2M, Marseille, France ³Materials Science Division, Argonne National Laboratory, 9700 South Cass Avenue, Argonne, Illinois 60439, USA ⁴Engineering Sciences and Applied Mathematics, Northwestern University, 2145 Sheridan Road, Evanston, Illinois 60202

To survive in harsh conditions, motile bacteria swim in complex environment and respond to the surrounding flow. Here we develop a mathematical model describing how the flagella bending affects macroscopic properties of bacterial suspensions. First, we show how the flagella bending contributes to the decrease of the effective viscosity observed in dilute suspension. Our results do not impose tumbling (random re-orientation) as it was done previously to explain the viscosity reduction. Second, we demonstrate a possibility of bacterium escape from the wall entrapment due to the self-induced buckling of flagella. Our results shed light on the role of flexible bacterial flagella in interactions of bacteria with shear flow and walls or obstacles.

Introduction

Bacteria being among the simplest living organisms, are the most abundant species on the planet. They significantly influence carbon cycling and sequestration, decomposition of biomass, transformation of contaminants in the environment. Trillions of symbiotic and pathogenic bacteria share human body space and form microbiota. Behavior of bacterial suspensions is an active topic of research¹⁻⁶. The recent discoveries include the onset of large-scale collective behavior^{2,3,7,8}, reduction of the effective viscosity⁹⁻¹¹, rectification of random motion of bacteria and extraction of useful energy¹²⁻¹⁴, enhanced mixing in bacterial suspensions^{1,15-17}.

Motile bacteria utilize bundled helical flagella to propel themselves in a fluid environment. Bacteria use the propensity to swim to search for food (e.g. chemotaxis), colonize new territory, or escape harsh conditions. Orientation of bacteria is also affected by shear flow, leading to a variety of non-trivial effects, such as rheotaxis (swimming against the flow)¹⁸ or depletion of bacterial concentration in shear flows^{5,19}. Unlike chemotaxis, i.e. drift along the concentration gradient, rheotaxis and concentration depletion are pure physical effects since no active receptor response is needed for the explanation of these phenomena. Elastomechanics of the bacteria, like bending and buckling of the flagella, could then play an important role in the understanding of these phenomena²⁰. A flagellum is, typically, at least, twice longer than the bacterial body and is flexible. Thus, flagella bending could result in a significant effect on bacterial trajectories²⁰⁻²³. Nonlinear dynamics of rigid microswimmers in two-dimensional Poiseuille flow were studied in Refs.^{24,25}. It was shown that the swimmers initially located away from channel walls exhibit a stable periodic motion around the centerline of the flow. Role of bacteria motility on zipping of individual flagellar filaments and formation of bacteria flagella bundle was investigated in Ref.²⁶. However, it was poorly understood how the flagellum can affect the bacterial dynamics due to bending in response to the

external shear flow or due to collision with the wall or obstacle. A model of a swimmer with flexible flagella in two fundamental shear flows, either planar shear or the Poiseuille flow in long channels, has been introduced in our previous work²⁷. A variety of surprising effects was discovered. For example, depending on the bending stiffness of the flagellum, the swimmer may migrate towards the center or exhibits periodic motion. This paper significantly extends and advances our results obtained in Ref.²⁷. Here we succeed to tackle two new important problems associated with the bacterial dynamics in shear flows. We show that flexibility of the bacterial flagella (i) contributes to the reduction of the effective viscosity and (ii) assists bacteria escaping entrapment near solid walls. Our results provide insight how microswimmers interact with external shear flow and with obstacles, realized, for example, in microfluidic devices or *in vivo*.

The first part of this work is motivated by the experimental observation in Ref.^{9,10} on the decrease of the effective viscosity of an active suspension of *B. subtilis*, in particular in the dilute regime, that is the volume fraction of bacteria is less than 1%. This result has been recently extended in Ref.¹¹ where a suspension of *E. coli* exhibited properties reminiscent that of a super-fluid: persistent flow and zero (or even negative) apparent viscosity. This is a hallmark of active matter: chemical energy stored in nutrient is turned into mechanical energy which is then used to counter-balance the viscous dissipation. Suspensions of active (self-propelled) swimmers representing bacteria were studied in Refs.^{19,28,29} and Ref.³⁰ with the primary goal to identify a mechanism resulting in the decrease of effective viscosity in a dilute regime. The works²⁸⁻³⁰ require bacteria to tumble (randomly change direction characterized by some tumbling rate or effective rotational diffusion D_r). Nevertheless, the strain of *B. subtilis* used in Ref.⁹ tumbles rarely, i.e. $D_r \ll 1$. Here we show that bacterial flagella bending contributes to the reduction of the effective viscosity even in the absence of tumbling. We derive an asymptotic expression for the effective viscosity for a dilute suspension. We show that this expression is in agreement with both the numerical solution of the model and qualitatively consistent with the experimental data from Ref.⁹.

The second and related part of the work focused on the bacterium behavior near surfaces (e.g. obstacles or walls). This problem naturally occurs in multiple setting relevant in biomedical context, e.g. formation of biofilms, migration of bacteria along channels, e.g., catheter, and industry (pipes clogging and biofouling). In many applications, bacteria swim in a confined container and their trajectory can be significantly affected by a nearby surface. Typically, bacteria are attracted by a no-slip surface (a wall) due to long-range hydrodynamic interactions³¹, then bacteria swim (mostly) parallel to the wall for a certain period of time. Eventually, bacteria can escape due to tumbling⁴ or can adhere to the wall. Study of behavior of flagellated swimmers near walls was initiated by Ref.³² where the accumulation of spermatozoa at the glass plates was documented. In the experimental works^{33,34} it was shown that *E. coli* is attracted by the wall and the straight trajectory becomes circular due to counter-rotation of bacterial body and the flagella. The tendency of bacteria to approach

the wall and to increase the curvature of their trajectory was observed by numerical modeling in Ref. ³⁵ where a bacterium was modeled as a sphere with helical flagella rotating with a constant angular velocity. To explain why the bacteria can swim near the wall adjacent to it for a long time, in Ref. ³⁶ authors hypothesized the presence of short-ranged forces of the van der Waals type. However, in Ref. ³⁷ by combining theory and experiment it was shown that van der Waals forces cannot be responsible for parallel swimming of the bacteria near wall. Instead authors proposed to extend the model from Ref. ³⁵ for a non-spherical bacterium body, and showed that bacteria may be kept at the wall by the additional torque caused by the non-sphericity. In addition to hydrodynamic attraction, bacteria can eventually re-orient themselves and swim away from the wall (escape). In Ref. ⁴ the time needed for bacteria to escape was estimated theoretically provided that rotational diffusion (for example, due to tumbling) is introduced. Authors ⁴ noted that even if bacteria do not tumble and are too large to be affected by thermal effects, the rotational diffusion can be assigned with a significant value due to noise in the swimming mechanism, whose essential constituent is flagellum dynamics. Here we consider how a bacterium that being initially entrapped and immobilized at a wall can escape exploiting its flagella flexibility. Such an entrapment may also naturally happen when the suspending liquid is anisotropic, e.g. lyotropic liquid crystal ^{38,39}. In this situation bacteria are swimming predominantly parallel to the average molecular orientation, i.e. liquid crystal director. In the case when the liquid crystal director is anchored perpendicular to the confining wall (homeotropic alignment), bacteria are forced to be aligned perpendicular to the wall and become trapped ^{38,40}. When the motility of bacteria is increased (by adding the oxygen), the bacterium may turn parallel to the wall due to the torque coming from the wall and the fact that forces which kept bacteria immobilized are small in compare to the self-propulsion (weak surface anchoring of the liquid crystal molecules). We show that a bacterium with rigid flagellum swims along the wall, so it stays essentially entrapped. In contrast, we show that a bacterium with flexible flagellum may rotate by an angle larger than $\pi/2$ and escape. This ability to escape reduces effects of bacteria on macroscopic properties of the suspension locally near the wall (due to decrease of bacterial concentration).

Model. In this work, we use a mathematical model in which a swimmer is evolving independently of the others. The model is referred to below as MMFS (the mathematical model of flagellated swimmer). The underlying physical assumptions of this model are the following: (i) the two-dimensional swimmer is composed of a rigid ellipse (body) and a flexible one-dimensional segment (flagellum); the flagellum is rigidly attached to the body (clamped); (ii) elastic and propulsion forces on the flagellum generate the thrust force which balances the drag force and leads to the motion of the swimmer; (iii) a propulsion force is uniformly distributed along the flagellum; (iv) background flow is not modified by the flagellum. The shape of the body (which is an ellipse) is described by parameter $\beta = \ell^2/(\ell^2 + d^2) = 1/2(1 - \epsilon^2)$ where ℓ and d are major and minor axes, respectively, and ϵ is the eccentricity of the ellipse. Small β corresponds to rod-like bodies, and $\beta = 1/2$ corresponds to spheres. The length of the flagellum, denoted by L , is assumed to be constant. The full list of parameters in the model as well as their typical values can be found in Table 2.

We stress here that a bacterial flagellum is a flexible helical filament which exhibits propeller-like motion by rotating around its helical axis and these rotations generate the propulsion force. In MMFS, this corresponds to that, according to (ii) above, the thrust force has two separate components: due to flagellum bending (the elastic force) and due to propulsion mechanism (the propulsion force). Moreover, a flagellum is modeled as a 1D (curved) segment in a plane with no helical structure, since the propulsion force already takes into account the helical structure of the flagellum and its axial rotation.

Given the initial state of the swimmer (orientation of the body and the shape of the flagellum at time $t = 0$), MMFS entirely determines the

state of the swimmer for all times $t > 0$. The unknown quantities of MMFS are the orientation of the body $\theta_0(t)$, the elastic stress of the flagellum $Q(s, t)$, and the tangential angle $\theta(s, t)$ of the flagellum at the point corresponding to arc length parameter s ; $s = 0$ is at the rigid interface body/flagellum and $s = L$ is at the free end of the flagellum. Using basic geometric formula, given $Q(s, t)$, $\theta(s, t)$, and $\theta_0(t)$, one can recover the trajectory of the swimmer, the shape and the location of every point of the flagellum $X(s, t) = (x(s, t), y(s, t))$. MMFS requires solving a coupled system of an ordinary differential equation for $\theta_0(t)$ and partial differential equations for $\theta(s, t)$ and $Q(s, t)$. The system is presented in electronic supplementary material; details on its derivation can be found in Methods. We analyze this system both numerically and using asymptotic expansions in the regime where the flagellum is almost rigid.

Results

Effective viscosity of a dilute suspension of flagellated swimmers.

A general formula for effective viscosity. Effective viscosity can be understood as a measure of the total shear stress of a suspension induced by a prescribed shear flow. In the context of bacterial suspensions, the stress resulting from the applied strain is due to the intrinsic resistance of suspending fluid and due to the stress created by the microswimmers (bacteria). In the dilute regime (small concentration), interactions between bacteria are negligible. Therefore, the superposition principle applies, that is the contribution to the total stress from all bacteria is the sum of the individual contributions. Moreover, due to their large number, each bacterium's contribution may be approximated in the sum by its expected value (taking a continuum limit). The dilute framework enables us to use MMFS to derive macroscopic properties of the suspension. Then the formula for the effective viscosity η_{eff} in a linear planar shear background flow of strain rate $\dot{\gamma}$ becomes ^{28,29,41-43}

$$\eta_{\text{eff}} = \eta_0 + \sum_{i=1}^n \eta_{\text{bact},i} \approx \eta_0 + n \int_0^{2\pi} \frac{\Sigma_{12}(\theta_0) + \Sigma_{21}(\theta_0)}{2\dot{\gamma}} P(\theta_0) d\theta_0, \quad (1)$$

where η_0 is the viscosity of the suspending fluid, $n = \Phi V_L$ is the number of particles in the volume V_L occupied by a suspension, Φ is the number density of bacteria, and the integral in the right hand side of Eq. (1) is the expected value of the contribution to the effective viscosity $\eta_{\text{bact},i}$ of the i th bacterium. The effective viscosity $\eta_{\text{bact},i}$ is the ratio between the anti-diagonal components Σ_{12} and Σ_{21} of the stress tensor Σ (induced by the bacterium) and the shear rate $\dot{\gamma}$. Here we assume that Σ_{12} and Σ_{21} are only determined by the angle orientation θ_0 of the bacterium. Thus, in order to compute the expected value of Σ_{12} and Σ_{21} , finding the distribution of orientation angles $P(\theta_0)$ is necessary.

MMFS is based on balance of forces and torques exerted by the swimmer on its rigid body surface and at each point of the flexible flagellum and the fluid drag forces and torques, respectively. Moreover, in MMFS the sum of forces exerted by the swimmer is zero. This is similar to the force-dipole model of a swimmer^{4,43} where the sum of the force that pushes the body in the fluid and the force that perturbs the fluid due to propulsion mechanism in the flagellum (represented in the force-dipole model by a point force exerted behind the body) is zero. The key difference between MMFS and the force-dipole model is that the sum of all torques exerted by the swimmer in MMFS is not necessarily zero, whereas for force-dipoles this sum is trivially zero. In particular, the force-dipole can not rotate if no external torque is exerted (a non-zero background flow, interactions with other swimmers, external magnetic field, etc.), while the flagellated swimmer may rotate if the flagellum is bent. The fact that the fluid balances a non-zero total torque exerted by the swimmer results in that, in general, the effective stress is non-symmetric in MMFS, i.e., $\Sigma_{12} \neq \Sigma_{21}$ ⁴⁴. Presence of a non-zero anti-symmetric part of the effective stress due to active contribution is the special feature of active chiral fluids⁴⁵.

In order to find Σ_{kl} one needs to solve the Stokes equation in the low Reynolds number regime: $-\nabla_{\mathbf{x}} \cdot \Sigma(\mathbf{x}) = F_{\text{bact}}(\mathbf{x})$, where Σ is the fluid

stress tensor, and F_{bact} is the bulk force due to the presence of the bacterium (the thrust force). Solving this equation is impractical due to the large domain of integration compare to the bacterium size. In a simpler model of a bacterium with rigid flagellum⁴³, each bacterium was approximated by a force dipole⁴ and the explicit expression for Σ is well-known in this case. Here our goal is to capture the effects coming from bending of elastic flagella in shear flow, so an approximation by the force dipole would oversimplify the consideration and would lead to zero net contribution to the effective viscosity. Instead, we use the Kirkwood approximation for the stress tensor^{46–48}

$$\Sigma_{kl} = \frac{1}{V_L} \int (F_{\text{bact}}(\mathbf{x}))_k (\mathbf{x} - \mathbf{x}_c)_l d\mathbf{x}, \quad (2)$$

where $F_{\text{bact}}(\mathbf{x})$ is non-zero in a small neighborhood of the center of mass of the bacterium \mathbf{x}_c , and V_L is the volume occupied by the fluid. The Kirkwood approximation can be also interpreted as the second term in the multi-pole expansion⁴².

In the context of MMFS (defined in the end of Introduction), $F_{\text{bact}}(\mathbf{x})$ is the sum of two forces distributed over the flagellum: (i) the uniform propulsion force $F_p \boldsymbol{\tau}(s)$ directed along the unit tangent vector $\boldsymbol{\tau}(s)$ with the magnitude F_p and (ii) the elastic force $Q(s) = \Lambda(s)\boldsymbol{\tau}(s) + N(s)\mathbf{n}(s)$ (Λ and N are tangent and normal components of Q , respectively). In the following, it will be convenient to separate contributions coming from propulsion and from elasticity for the components of the stress tensor: $\Sigma_{kl} = \Sigma_{kl}^{\text{propulsion}} + \Sigma_{kl}^{\text{elastic}}$, where according to the formula (2)

$$\begin{aligned} \Sigma_{kl}^{\text{propulsion}} &= \frac{1}{V_L} \int_0^L F_p \tau_k(s) (X_l(s) - X_l(0)) ds, \\ \Sigma_{kl}^{\text{elastic}} &= \frac{1}{V_L} \int_0^L \frac{\partial Q_k}{\partial s}(s) (X_l(s) - X_l(0)) ds, \end{aligned} \quad (3)$$

and analogously for the effective viscosity η_{eff} :

$$\frac{\eta_{\text{eff}} - \eta_0}{\eta_0} = \eta_{\text{propulsion}} + \eta_{\text{elastic}}, \quad (4)$$

where each of the two terms is computed via (3) and (1).

Terms in the right hand side of (4) take into account the effect of the flagellum. This means that the contribution to the effective viscosity due to presence of rigid ellipsoidal bodies in the fluid is included in η_0 . In other words, η_0 is the effective viscosity of the dilute suspension of rigid ellipsoids and $\eta_0 \approx \eta_{\text{fluid}} [1 + \nu\Phi]$, where η_{fluid} is the viscosity of water, Φ is the number density. The formula for the coefficient ν is well-known: for spheres $\nu = 2.5$ (the Einstein's formula⁴⁹), for ellipsoids the formula for ν was obtained by Jeffery (formulas (62) and (64) in Ref.⁵⁰).

Asymptotic results for large bending stiffness of flagellum. We present here our results on computations of $\eta_{\text{propulsion}}$ and η_{elastic} as functions of the following geometrical and physical dimensionless parameters: shape parameter β (describes shape of the bacterium body; $\beta = 0$ for needles and $1/2$ for spheres), ratio of bacterial body length to the flagella length $r = \ell/L$ (ℓ and L are the body and the flagellum length, respectively), and the compound dimensionless parameter characterizing ratio of drag force to elastic force $\varepsilon = L^4 \dot{\gamma} \zeta_b / K_b$ (ζ_b is the drag coefficient and K_b is the bending stiffness of the flagellum). We use two scale asymptotic expansions in small ε (stiff flagella) to establish explicit expression for the effective viscosity η_{eff} . Note that for fixed values of ζ_b , L and $\dot{\gamma}$, taking ε small is equivalent to the limit as flagellum is nearly rigid. That implies that the bending stiffness of the flagellum K_b is large (the reader should not be confused by the fact that the typical K_b we use for bacteria and call it "large" is of the order $10^{-23} \text{ N}\cdot\text{m}^2$; after nondimensionalization K_b is replaced by ε^{-1} , for details see electronic supplementary material, section 2). Necessity of two scales in the asymptotic expansions in the "rigid" limit is explained by the two different time scales for dynamics of the smoothly translating bacterial body and rapidly oscillating flagellum.

The two scale asymptotic expansion methods for equations of MMFS (see supplementary material, section 2, for a description of the method) is used to derive the following asymptotic expression for the tangential and normal components of the elastic stress: $\Lambda(s) = p_\Lambda(s) \sin 2\theta_0 - \frac{F_p(s-L)}{1+k_r}$, $N(s) = p_N(s) \cos 2\theta_0$. Polynomials $p_\Lambda(s)$ and $p_N(s)$ are of the second order with respect to arc length s with coefficients proportional to ζ_b and $\dot{\gamma}$ and they also depend on shape parameter β , flagellum length L , body length ℓ and drag coefficient k_r (see Table 2 with the list of parameters). The second term in the expression for the tangential component of the elastic stress is due to the propulsion force which acts in the tangential direction $\boldsymbol{\tau}$ with the strength F_p . We also found the asymptotic expression for the flagellum shape described by the slope angle: $\theta(s) = \theta_0 + \varepsilon p_\theta(s) \cos 2\theta_0$, where $p_\theta(s)$ is a polynomial of the fourth order with respect to arc length s and coefficients depending on β , ℓ , L , k_r . Details of derivation of expressions for Λ , N and θ with explicit formulas for coefficients of polynomials p_Λ , p_N , and p_θ can be found in the electronic supplementary material.

The distribution of orientation angles $P(\theta_0)$ from Eq. (1) is in general a function of both angle of the body θ_0 and time t , and satisfies the Liouville continuity equation

$$\begin{cases} \frac{\partial}{\partial t} P(\theta_0, t) + \frac{\partial}{\partial \theta_0} \left[\frac{1}{\zeta_r} (\text{T}_{\text{shear}} + \text{T}_{\text{flagellum}}) P(\theta_0, t) \right] = 0, \\ \int_0^{2\pi} P(\theta_0, t) d\theta_0 = 1, \end{cases} \quad (5)$$

where T_{shear} and $\text{T}_{\text{flagellum}}$ are torques exerted on the ellipsoidal body of the bacterium by the background shear flow and by the flagellum, respectively. Parameter ζ_r is the rotation drag coefficient, and $\frac{1}{\zeta_r} (\text{T}_{\text{shear}} + \text{T}_{\text{flagellum}})$ is the angular velocity of the body caused by shear and flagellum. It is well-known⁴² that T_{shear} can be explicitly written as a function of θ_0 :

$$\begin{aligned} \text{T}_{\text{shear}} &= -\dot{\gamma} \zeta_r ((1 - \beta) \sin^2 \theta_0 + \beta \cos^2 \theta_0) \\ &= -\frac{\dot{\gamma} \zeta_r}{2} (1 - (1 - 2\beta) \cos 2\theta_0). \end{aligned} \quad (6)$$

Equality $\zeta_r \frac{d\theta_0}{dt} = \text{T}_{\text{shear}}(\theta_0)$ is known as the Jeffery equation for rotating ellipses in the shear flow^{42,50}. In order to compute $\text{T}_{\text{flagellum}} = \frac{\ell}{2} N|_{s=0}$, one needs to solve the elasticity equations for the flagellum. However, using the asymptotic method it is possible for $\varepsilon \ll 1$ to represent $N|_{s=0}$ (and, thus, $\text{T}_{\text{flagellum}}$) as a function of θ_0 , which turns Eq. (5) in a closed form. The resulting equation is the same as the Jeffery equation for ellipses with the effective shape parameter $b = \frac{r\beta}{1+2r}$ in place of β . In other words, an ellipse with the rigid flagellum has same trajectories as the more prolate ellipse with no flagellum. The equilibrium distribution which satisfies Eq. (5) for $\varepsilon \ll 1$ is given by

$$P(\theta_0) = \frac{q}{2\pi} \frac{1}{1 - (1 - 2b) \cos(2\theta_0)}, \quad (7)$$

where $q = \sqrt{1 - (1 - 2b)^2}$; constant $q/2\pi$ is introduced, so $P(\theta_0)$ satisfies the normalization condition in (5). Since the effective viscosity should be a property of the suspension independent of time and all solutions of Eq. (5) for $\varepsilon \ll 1$ converges to the equilibrium distribution (if one assumes a small rotational diffusion), we use $P(\theta_0)$ from Eq. (7) when apply Eq. (1).

Substituting the asymptotic expansions into formula (1), the effective viscosity of the dilute suspension of flagellated swimmers is expressed as

$$\frac{\eta_{\text{eff}} - \eta_0}{\eta_0} = \Phi \frac{L^3}{\eta_0} Z_{\text{elastic}}(\beta, r) - \Phi \varepsilon \frac{F_p L^2}{\eta_0 \dot{\gamma}} Z_{\text{prop}}(\beta, r), \quad (8)$$

where Φ is the number density of bacteria in the suspension and expressions for elastic and propulsion contribution coefficients Z_{elastic} and Z_{prop} can be found in the electronic supplementary material, section 2.5; both

Z_{elastic} and Z_{prop} are positive. We point out here that Eq. (8) implies that the change of the effective viscosity is obtained by the interplay between elastic and propulsion contributions. Namely, whatever the parameters β and r are, the propulsion decreases the viscosity, whereas the elastic part of the stress tends to increase the viscosity (see Figure 1). For small r (i.e. long flagella), the propulsion contribution coefficient Z_{prop} behaves as $1/r^5$ whereas the elastic contribution coefficient Z_{elastic} behaves as $1/(r^2 \log(r))$. This implies that for r small enough, the propulsion should dominate elasticity.

In order to present quantitative results on the effective viscosity obtained by two scale asymptotic expansions, consider a dilute suspension with the volume fraction of bacteria about 1%. The total force generated by the flagellum is about 10 pN, and the typical size of the flagellum is about 10 μm , which makes the propulsion strength equal to $10^{-11} \cdot 10^{-5} = 10^{-16} \text{ N} \cdot \text{m}$. The suspending fluid is taken to be water ($\eta_0 = 10^{-3} \text{ Pa} \cdot \text{s}$). A realistic value of the bending stiffness of the flagellum is $K_b = 3 \cdot 10^{-23} \text{ N} \cdot \text{m}^2$ (⁵¹) and shear rate $\dot{\gamma} = 0.1 \text{ s}^{-1}$, the parameter $\varepsilon = 0.03$. The values of η_{eff} computed by (8) is depicted in Figure 1.

Certain flagellated bacteria have the ability to swim through environments of relatively high viscosity ⁵²⁻⁵⁴. Then the bacteria can maintain an almost constant speed whatever the fluid resistance they encounter. In the first approximation, the velocity of the swimmer $\sim F_p/\eta_0$, then bacteria can increase their propulsion force while surrounded by a more viscous fluid. In such a fluid ($\eta_0 = 5 \cdot 10^{-3} \text{ Pa} \cdot \text{s}$ and $F_p = 1.5 \mu\text{N} \cdot \text{m}^{-1}$), we predict a decrease of viscosity for $r < 0.55$ ($r = 0.5$ for *B. subtilis*) (Figure 1, c). For higher values of the shape constant β , the decrease of effective viscosity also occurs for shorter flagella (Figure 1, (d)).

Numerical simulations. We performed computational analysis of MMFS and computed the effective viscosity η_{eff} as well as propulsion and elastic contributions $\eta_{\text{propulsion}}$ and η_{elastic} . The expected value integral in the right hand side of Eq. (1) was approximated by the time average of its integrand.

For large K_b (small ε), the results of numerical solution are in a good agreement with asymptotic expression Eq. (8) (see Figure 1 and the Table 1). Note that the asymptotic parameter ε is proportional to L^4 , so the agreement between numerical and asymptotic solution is lost for small r (long flagellum). The set of values of the flagellum length L for which the decrease of viscosity is observed depends on the bending stiffness K_b . Table 1 compares results of asymptotic approach and numerical solution, the threshold values of L , r and ε needed to have a decrease of viscosity are given.

For the following model parameters: $K_b = 3 \cdot 10^{-23} \text{ N} \cdot \text{m}^2$, $\eta_0 = 10^{-3} \text{ Pa} \cdot \text{s}$, $L = 12 \mu\text{m}$ and $F_p = 1.5 \mu\text{N} \cdot \text{m}^{-1}$, asymptotic and numerical values of η_{eff} are in agreement with experiment ⁹, i.e. we predict a decrease of effective viscosity of $\approx 10\%$ for the number density of $\Phi = 5 \cdot 10^9 \text{ cm}^{-3}$ (see the first part, $\Phi < 10^9 \text{ cm}^{-3}$, of the curve in Figure 3 in Ref. ⁹).

Flagellated swimmers can escape from the wall. Here we consider how flagella flexibility assists the bacterium to escape from the wall. A swimmer can be entrapped by a wall such that its orientation is perpendicular to the wall. This kind of entrapment may happen, for example, in lyotropic (water soluble) nematic liquid crystal with the homeotropic surface anchoring ^{38,40} (the liquid crystal director is perpendicular to the wall): since the bacteria tend to align with the nematic director, they eventually become perpendicular to the wall (for simplicity we neglect here the effects associated with the anisotropic elastic and viscous torques exerted by the liquid crystal on a bacterium). Moreover, motile bacteria would hit the wall. However, due to flagella rotation and bending, this perpendicular alignment may become unstable.

Settings of the problem are as follows. Bacterium's body initially has the orientation $\theta_0 = \pi$, that is, the body is oriented horizontally, pointing to the right, at the vertical wall $x = 0$. Flagellum is initially slightly perturbed from a straight configuration (while unstable, perfectly straight

flagellum will lead to no motion). Bacterium's body experiences three torques: (i) due to the flagellum, applied at the point of its attachment to the body, (ii) due to the wall, applied at the point of touching the wall (if the body does not touch the wall, then this torque is 0), and (iii) due to the surrounding viscous fluid (see Figure 2, (a)).

We use MMFS with a modification to take into account the additional torque when the swimmer is touching the wall. A variety of nontrivial swimming regimes was numerically observed depending on the values of the bending stiffness of the flagellum, K_b , all other parameters being fixed, their values can be found in Table 2. Numerical analysis shows that qualitative behavior of the swimmer depends on the bending stiffness of the flagellum, K_b . If $K_b < 5 \cdot 10^{-24} \text{ N} \cdot \text{m}^2$ ("soft" flagellum) the swimmer rotates and swims parallel to the wall. Thus, in this case, though the swimmer is not immobilized at the wall, it is still entrapped by the wall and cannot escape. For $5 \cdot 10^{-24} \text{ N} \cdot \text{m}^2 < K_b < 2.2 \cdot 10^{-23} \text{ N} \cdot \text{m}^2$, the swimmer eventually swims away from the wall, hence showing ability to escape due to the flagellum. For the large bending stiffness, $K_b > 2.2 \cdot 10^{-23} \text{ N} \cdot \text{m}^2$ ("almost rigid" flagellum), as it is expected for the rigid flagellum, swimmer rotates by $\pi/2$ and then swims parallel to the wall (see Fig. 2, (b) and (c), and the electronic supplementary material, videos S1–S4). The difference between "soft" and "almost rigid" cases is that in the first one the body exhibits visible oscillations, whereas in the latter, it swims straight parallel to the wall. This non-trivial qualitative behavior of the swimmer depending on K_b is also observable when no obstacle is present in the fluid. Regardless initial shape the swimmer eventually either orients itself toward one direction and swims straight or exhibits periodic oscillations (see Figure 2, (d) for the case with no background flow; more complicated dependence on K_b of large time behavior of the swimmer was observed in the Poiseuille flow, see Figure 3 (e) in Ref.²⁷; see also the electronic supplementary material, video S5). These differences in qualitative behavior may serve as a basis to isolate bacteria with bending stiffness in a given range (or equivalently, different numbers of flagella since effective K_b is proportional to the number of flagella).

Discussion

We provide a heuristic explanation why the flagellum helps decrease the viscosity. For the illustration we will use the force dipole representation of a bacterium, that is, the representation by two forces of equal magnitude and opposite directions. In work ⁴ it was shown experimentally that the flow from a swimming bacterium is well approximated by the flow generated by a force dipole. Above we mentioned that such a representation is not sufficient for our purposes to study the impact of flexible flagellum. However, for the sake of simplicity the force dipole model is sufficient if we allow the dipole not to be straight: the line connecting points where two opposite forces are exerted is not necessarily parallel to these forces (see Figure 3, right).

The key point is that the orientation of the dipole created by each swimmer is modified by the presence of the flagellum, which, in turn, affected by the shear flow. The shape of the flagellum is plotted in Figure 3. Two mechanisms are responsible for the shape of the flagellum. First, the fluid has a direct action on the flagellum. This effect is prevalent when the flagellum is perpendicular to the fluid ($\theta_0 = \frac{\pi}{2}$ in Figure 3). When the flagellum is oriented in the direction of the flow, this effect tends to become negligible. Second, the rotation of the body makes one of the end of the flagellum (the end attached to the body) move faster than the other, which also modifies the shape of the flagellum. This effect is prevalent for $\theta_0 = 0$ in Figure 3.

Given that a dipole oriented a $\pi/4$ or $5\pi/4$ helps the fluid to flow, and that a dipole oriented a $3\pi/4$ or $7\pi/4$ prevents the fluid to flow, the symmetry in the body orientation distribution leads to no decrease of viscosity. The flagellum breaks the symmetry in the dipole orientation, for example, a body oriented at $\pi/2$ (neutral for η_{eff} without flagellum) creates a dipole oriented close to $\pi/4$ thanks to the flagellum. As a result, in average, the

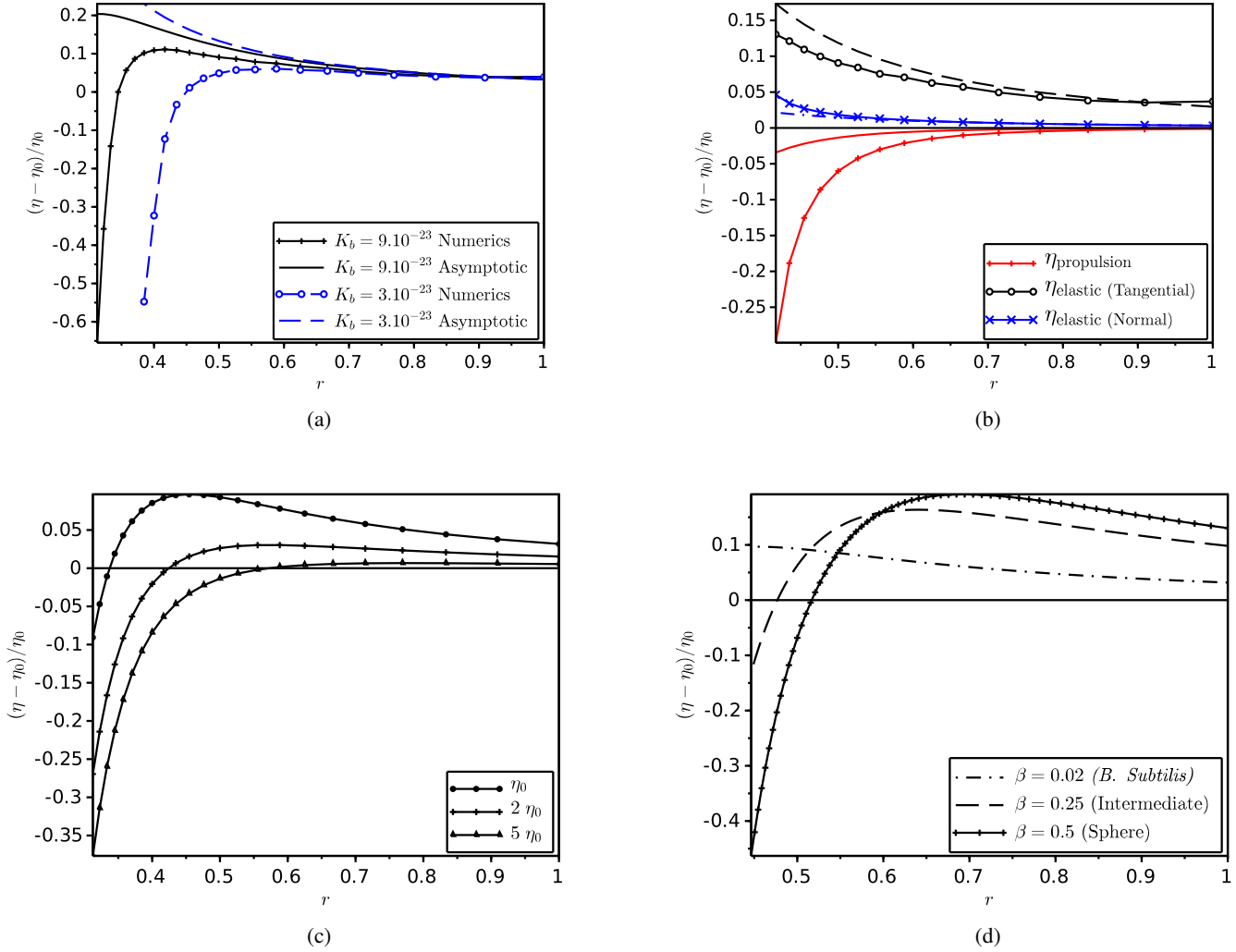


Figure 1 | Effective viscosity as a function of model parameters. (a) Comparison of effective viscosity change obtained by two scale asymptotic expansions and numerical simulations for $K_b = 3 \cdot 10^{-23}$ N · m² (black) and $K_b = 9 \cdot 10^{-23}$ N · m² (blue) and various r ; (b) Contributions from propulsion and elasticity (both tangential and normal components) for $K_b = 3 \cdot 10^{-23}$ N · m² are shown. (c) Effective viscosity η_{eff} for various fluid viscosities η_0 . (d) Effective viscosity vs the body shape constants β .

orientation helping the fluid to flow are more likely than the others.

We point out that in contrast with the work⁴³, the propulsion contribution to η_{eff} has no apparent singularity for the strain rate $\dot{\gamma} = 0$ (which is regularized by an infinitesimal rotational diffusion), and in the first approximation (rigid flagellum) it does not depend on the shear rate. This singularity is regularized because the non dimensional parameter ε is proportional to $1/\dot{\gamma}$. The bulk stress depends on how much the flagellum bends, which is in the first approximation directly proportional to the bulk rate of strain. As a result, the shear rate modifies linearly the propulsion stress, then their ratio is constant in $\dot{\gamma}$: as $\dot{\gamma} \rightarrow 0$ (and, thus, $\varepsilon \rightarrow 0$), the propulsion contribution to the effective viscosity equals to $-\Phi \frac{L^6 \zeta_b F_p}{K_b} Z_{prop}(\beta, r)$ (the expression for the non-dimensional parameter $Z_{prop}(\beta, r)$ can be found in the electronic supplementary material, section 2.5). Thus, the small strain rate $\dot{\gamma}$ limit is well-defined, and leads to a specific value of the effective viscosity even in the absence of fluctuations. This result is in agreement with the experiment¹¹ where a well-defined value of effective viscosity was observed for very small shear rates.

Conclusions

In this work we demonstrated how flexibility of bacterial flagella affects macroscopic properties of the suspension of microswimmers. We found that flagella bending may lead to a decrease of the effective viscosity in the absence of random reorientations. This effect is amplified with the increase in the viscosity of suspending fluid since many bacteria often increase their propulsion force⁵²⁻⁵⁴. Moreover, we show that flagella buckling may assist bacteria to escape entrapment at the wall. Our findings highlight the wealth of new intriguing phenomena stemming from the flexibility of the swimmer's body that include reduction of the viscosity, escape from the wall entrapment, migration towards flow centerline and many others.

In the course of our work we approximated helical flagella by an elastic beam with the propulsion force distributed uniformly along the beam. Obviously, this approximation neglects intrinsic chirality of the flagella, which leads to its clockwise rotation and counter-clockwise rotation of the head. The chirality of the flagellum can be responsible for such phenomena as rheotaxis¹⁸ and circular motion near the wall³⁴. Incorporating flagella chirality into our analysis would be desirable, but technically challenging. We anticipate that the torques arising from the helical shape of the flagellum are negligible compared to the bending stresses considered

| | $K_b=3 \cdot 10^{-23} \text{ N} \cdot \text{m}^2$ | | $K_b=9 \cdot 10^{-23} \text{ N} \cdot \text{m}^2$ | |
|--|---|----------------------|---|----------------------|
| | Asymptotics | Numerics | Asymptotics | Numerics |
| $\frac{\eta_{\text{eff}} - \eta_0}{\eta_0} < 0$ | $L > 15 \mu\text{m}$ | $L > 11 \mu\text{m}$ | $L > 22 \mu\text{m}$ | $L > 15 \mu\text{m}$ |
| | $r < 0.33$ | $r < 0.45$ | $r < 0.23$ | $r < 0.34$ |
| | $\varepsilon > 0.16$ | $\varepsilon > 0.05$ | $\varepsilon > 0.24$ | $\varepsilon > 0.05$ |
| $\frac{\eta_{\text{eff}} - \eta_0}{\eta_0} < 10\%$ | $L > 16 \mu\text{m}$ | $L > 12 \mu\text{m}$ | $L > 23 \mu\text{m}$ | $L > 16 \mu\text{m}$ |
| | $r < 0.31$ | $r < 0.43$ | $r < 0.22$ | $r < 0.32$ |
| | $\varepsilon > 0.21$ | $\varepsilon > 0.06$ | $\varepsilon > 0.26$ | $\varepsilon > 0.06$ |

Table 1 | Comparison of numerical solution with the asymptotic results

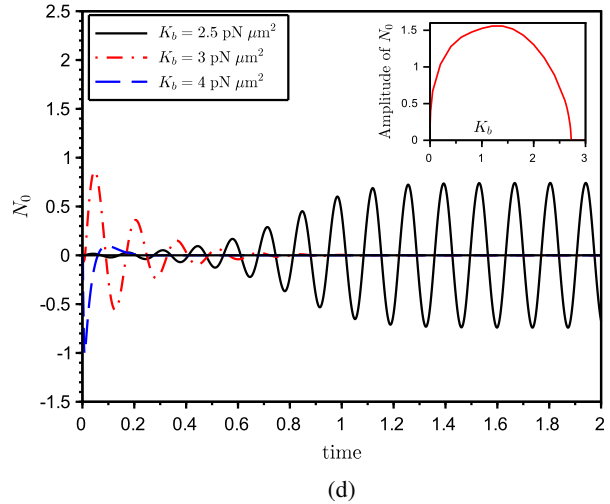
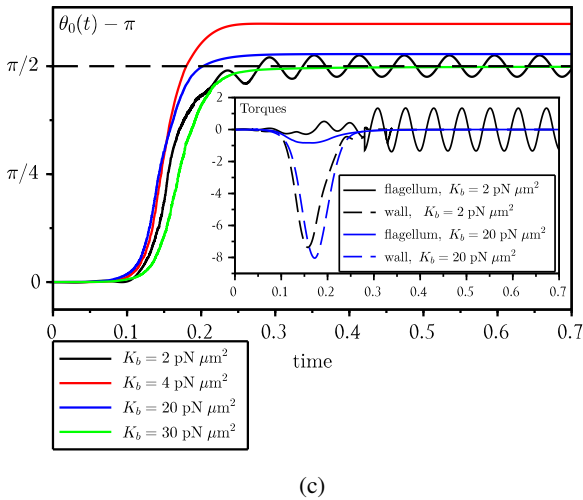
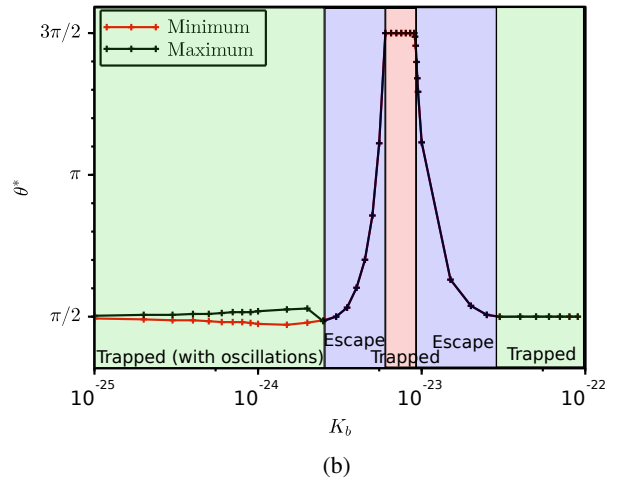
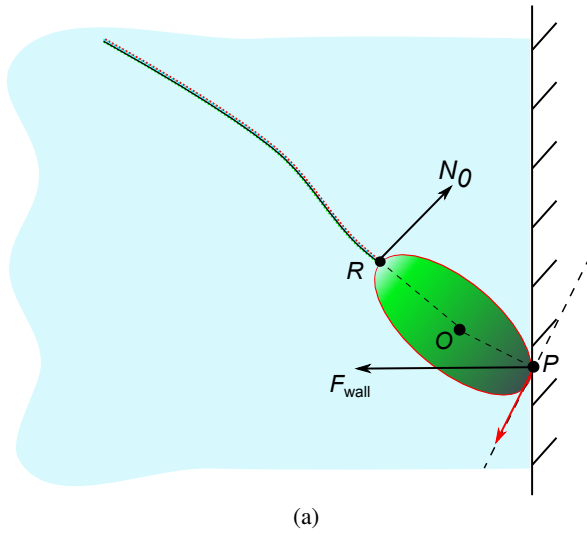


Figure 2 | **Escape from the wall.** (a) Bacteria at the wall (sketch). Body is an ellipsoid centered at point O ; the ellipsoid touches the wall at point P ; flagellum is rigidly attached to the body at point R . Three forces act on the body: the normal force coming from flagellum N_0 , the wall reaction F_{wall} , and the fluid over the boundary of the ellipsoid. Red arrow stands for the component of F_{wall} contributing to the torque. The light blue zone represents the domain with fluid. (b) The plot demonstrates how qualitative behavior of an initially entrapped swimmer depends on flagellum bending stiffness K_b : the swimmer either remains trapped (red and green zones), or eventually escapes with a limiting angle from $(\frac{\pi}{2}, \frac{3\pi}{2})$ (blue zone); θ^* (vertical axis) denotes the orientation of the swimmer for large times, $t \gg 1$. (c) Evolution of the orientation angle (main plot) and torques due to flagellum and the wall (inset). A bacterium swims towards the wall and touches it at time $t \approx 0.1$. When the bacterium body touches the wall, the torque due to the wall becomes non-zero. (d) The plot depicts dynamics N_0 for various K_b of the swimmer in the fluid with no obstacles and no background flow (the plot for $K_b = 4 \cdot 10^{-24} \text{ N} \cdot \text{m}$ is magnified by a factor 200 for better visibility); three plots demonstrate that depending on K_b the swimmer eventually exhibits oscillations with constant or decaying amplitude or N_0 converges to 0 with no oscillations. Inset: the plot demonstrates the dependence on K_b of the amplitude of N_0 when the swimmer exhibits oscillations.

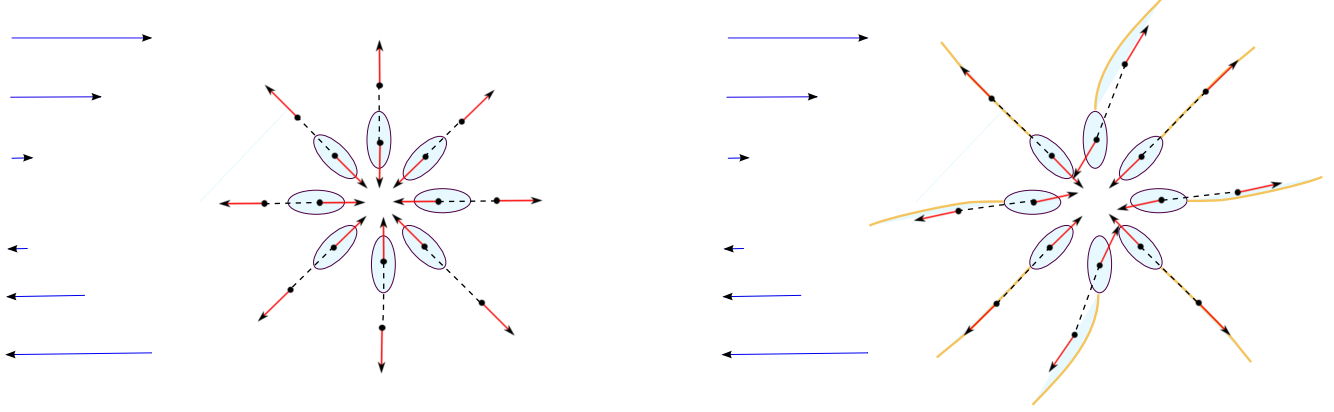


Figure 3 | Illustration of the viscosity reduction due to flagella bending. In red: Dipole exerted by the swimmer on the fluid, for different body orientations $i\pi/4$, $i = 0 \dots 7$. (a) rigid flagellum. (b) elastic flagellum. The shape of the flagellum is obtained from the analytic formula provided by two scale asymptotic expansion.

here, and, thus, do not affect the phenomena considered in this work (see the electronic supplementary material, section 3).

METHODS

We use an extension of the model of the flagellated swimmer from Ref.²⁷. The model is two-dimensional and describes the swimmer as a rigid body of an ellipsoidal shape with an attached elastic beam representing the flagellum (see Supplementary Figure 1). The orientation of the swimmer θ_0 is defined as the orientation of the principal axis of the body with respect to horizontal, and the equation for θ_0 is derived from the torque balance:

$$\zeta_r \omega = T_{\text{shear}} + T_{\text{flagellum}} + T_{\text{external}}. \quad (9)$$

The equation reads as follows. The viscous torque which is linearly proportional to the angular velocity of the body $\omega = \frac{d\theta_0}{dt}$ is balanced by the torques coming from the shear flow, flagellum, and possible external torque (for example, due to the presence of a wall). Equation (9) is a modification of the well-known Jeffery equation for rotating ellipsoids in a background shear flow^{42,50}.

The flagellum is a segment of a curve of the constant length L and with arc-length parameter s , $0 \leq s \leq L$. Unit vectors $\boldsymbol{\tau}(s)$, $\mathbf{n}(s)$ and $\mathbf{b}(s)$ represent tangent, normal and bi-normal vectors of the curve, respectively. Within the flagellum, the viscous (drag) force is balanced by the propulsion and elastic forces:

$$\mathbf{F}_{\text{drag}}(s) = \mathbf{F}_{\text{propulsion}}(s) + \mathbf{F}_{\text{elastic}}(s). \quad (10)$$

The propulsion force is assumed to have a constant magnitude and to be always exerted in the tangent direction: $\mathbf{F}_{\text{propulsion}} = F_p \boldsymbol{\tau}$. The elastic force is given by the internal stress $Q(s)$ which is the force exerted by the segment $[s, L]$ of the flagellum on the segment $[0, s]$. Thus, $\mathbf{F}_{\text{elastic}} = -\frac{\partial Q}{\partial s}$. Elasticity of flagellum is constituted through the relation for internal torque $\mathbf{M}(s) = \boldsymbol{\tau}(s) \times \mathbf{F}_{\text{elastic}}(s)$:

$$\mathbf{M}(s) = K_b \kappa(s) \mathbf{b}(s), \quad (11)$$

which reads that \mathbf{M} is proportional to the bending stiffness K_b and to the local curvature of the flagellum κ . One end, $s = 0$, is rigidly attached to the body (clamped), and another end, $s = L$, is free and the flagellum is straight there: $Q(L) = \kappa(L) = 0$. The propulsion is transmitted to the body, thus, pushing the swimmer forward, through the point of junction and is present in the force balance equation for the body

$$\zeta_b V = \mathbf{F}_{\text{propulsion}}(0) + \mathbf{F}_{\text{elastic}}(0), \quad (12)$$

where $\zeta_b V$ is the drag force for the body and, by the Stokes law, it is proportional to the body velocity V with a drag coefficient ζ_h .

After proper rewriting, all the above equations (9), (10), (11), (12) result into a coupled system of an ordinary differential equation for the body, non-linear elliptic partial differential equation of the second order for the tangential

component of Q , highly nonlinear parabolic partial differential equation of the fourth order for the shape of the flagellum, and certain boundary conditions. The system is written in the electronic supplementary material, section 1.

The system provides a deterministic description of an isolated swimmer, given its initial position, shape and orientation. Swimming can be defined⁵⁵ as the ability to advance in a fluid in absence of external propulsive forces, by performing cyclic shape changes. Specifically, we can define a low-Reynolds swimmer as an object which can modify, via an intrinsic mechanism (cyclic change of shape, rotation of an helix) the fluid velocity around itself, which leads to the creation of a propulsion force responsible for a net displacement of the center of mass. For instance, *B. subtilis* actuate passive helical filaments (the flagella) using rotary motors embedded in the cell walls, and whose rotation gives rise to propulsion. This is made possible because the flagellum is an helix undergoing a drift across streamlines due to its chirality⁵⁶, as opposed to rods undergoing classical Jeffery orbits⁴². The non-symmetry in the chirality force breaks the scallop theorem⁵⁷.

In the derivation of the system, the following major simplifications were made. First, although the three-dimensionality of the helix is crucial for motion, the model we consider is two-dimensional, and we represent the 3D chiral force by a propulsion force density uniformly applied along the flagellum. Second, the drag force acting on the swimmer is given by the fluid velocity relative to the swimmer velocity. This means that the local effects on the fluid in the neighborhood of the swimmer are not described. Such an approach is justified because we only consider dilute suspensions (the other swimmers are far). We also note here that somewhat similar model was considered in Ref.⁵⁸ to study magneto-elastic filaments. We conclude this section with the list of parameters used in the paper, see Table 2.

Acknowledgements The work of M.T., M.P. and L.B. was supported by the NIH grant 1R01GM104978-01. The research of I.S.A. was supported by the US Department of Energy (DOE), Office of Science, Basic Energy Sciences (BES), Materials Science and Engineering Division.

Contributions M.P., M.T., L.B. and I.S.A. designed and performed the study and wrote the paper. M.P. and M.T. contributed equally to this work.

Competing Interests The authors declare that they have no competing financial interests.

Correspondence Correspondence and requests for materials should be addressed Igor S Aranson (email: aranson@anl.gov).

| parameter | typical value | description |
|----------------|---|---|
| L | $1.2 \cdot 10^{-5}$ m | flagellum length |
| ℓ | $0.5 \cdot 10^{-5}$ m | body length (major axis of ellipse) |
| d | $7 \cdot 10^{-7}$ m | body thickness (minor axis of ellipse) |
| β | 0.0162 | body shape parameter, $\frac{d^2}{\ell^2 + d^2}$ |
| $\dot{\gamma}$ | 0.1 s ⁻¹ | shear rate |
| η_0 | 10^{-3} Pa s | viscosity of the surrounding fluid |
| F_p | 10^{-7} N m ² | propulsion force |
| K_b | $3 \cdot 10^{-23}$ N m ² | flagellum bending stiffness |
| ζ_b | 10^{-3} N s m ⁻² | drag coefficient per unit length for the flagellum |
| ζ_h | $1.6 \cdot 10^{-8}$ N s m ⁻¹ | drag coefficient for the body |
| ζ_r | $6.7 \cdot 10^{-20}$ N s m | rotational drag coefficient for the body |
| α | 2 | drag anisotropy factor (ratio tangential/normal force needed to drag flagellum point) |
| k_r | 0.65 | $L\zeta_b/\zeta_h$ (auxiliary parameter) |
| r | 0.41 | ℓ/L |
| ε | 0.07 | $L^4\dot{\gamma}\zeta_b/K_b$ |

Table 2 | Main model parameters

A MMFS - Mathematical Model of Flagellated Swimmer In this supplementary section, we explain how the trajectory of the swimmer and the dynamics of its flagellum are computed in the framework of MMFS. Recall that the swimmer consists of a rigid body and a flexible flagellum (see Fig. 4).

The body is an ellipse centered at $X^b(t) = (x^b(t), y^b(t))$ with the major and minor axes ℓ and d , respectively. The swimmer swims in the background flow u^{BG} (either the shear flow $u^{\text{BG}}(x, y) = (-\dot{\gamma}y, 0)$ or zero flow $u^{\text{BG}} = (0, 0)$). The body velocity $V^b(t) = \frac{dX^b(t)}{dt}$ is given by

$$V^b(t) = u^{\text{BG}}(X^b(t)) + \frac{1}{\zeta_b} \left\{ \Lambda(0)\boldsymbol{\tau} + \frac{1}{\alpha}N(0)\mathbf{n} \right\}. \quad (13)$$

Equation (13) reads as follows: relative velocity of the body with respect to background flow is determined by the force exerted by the flagellum (Stokes law); the parameter α takes into account that the ability of the flagellum to drag the body (or, the ability to affect the body velocity) in normal and tangent directions are different, $\alpha \neq 1$. Recall that $Q(s) = \Lambda(s)\boldsymbol{\tau} + N(s)\mathbf{n}$ is the elastic stress, that is the force exerted by the segment $[s, L]$ of the flagellum on the segment $[0, s]$.

The flagellum location $X(s, t) = (x(s, t), y(s, t))$ as a function of the body location $X^b(t) = (x^b(t), y^b(t))$ and flagellum orientation $\theta(s, t)$ is given by the geometrical relations

$$\begin{cases} x(s, t) = x(0, t) + \int_0^s \cos(\theta(z, t))dz, & y(s, t) = y(0, t) + \int_0^s \sin(\theta(z, t))dz, \\ x(0, t) = x^b(t) + \frac{\ell}{2} \cos(\theta_0(t)), & y(0, t) = y^b(t) + \frac{\ell}{2} \sin(\theta_0(t)). \end{cases} \quad (14)$$

In order to find $\theta(s, t)$, $\theta_0(t)$, $\Lambda(s, t)$ and $N(s, t)$, the following PDE/ODE system is considered. It consists of an ODE for body orientation angle $\theta_0(t)$, a parabolic forth-order PDE for flagellum orientation angle $\theta(s, t)$, and an elliptic second order PDE for the tangential elastic stress $\Lambda(s, t)$. Independent variables are $t > 0$ and $0 < s < L$.

$$\frac{d\theta_0}{dt} = -\dot{\gamma} \left((1 - \beta) \sin^2 \theta_0 + \beta \cos^2 \theta_0 \right) + \frac{\ell}{2\zeta_r} N(0, t), \quad (15)$$

$$\frac{\partial \theta}{\partial t} = -\frac{K_b}{\alpha \zeta_f} \frac{\partial^4 \theta}{\partial s^4} + \frac{1}{\zeta_f} \left(\frac{1}{\alpha} \Lambda + K_b \left(\frac{\partial \theta}{\partial s} \right)^2 \right) \frac{\partial^2 \theta}{\partial s^2} + \frac{1}{\zeta_f} \left(\frac{\alpha + 1}{\alpha} \frac{\partial \Lambda}{\partial s} + F_p \right) \frac{\partial \theta}{\partial s} - \dot{\gamma} \sin^2(\theta), \quad (16)$$

$$\frac{\partial^2 \Lambda}{\partial s^2} = \frac{1}{\alpha} \left(\frac{\partial \theta}{\partial s} \right)^2 \Lambda - K_b \left(\frac{\partial^2 \theta}{\partial s^2} \right)^2 - \frac{\dot{\gamma} \zeta_f}{2} \sin(2\theta) - \frac{(\alpha + 1)}{\alpha} K_b \frac{\partial^3 \theta}{\partial s^3} \frac{\partial \theta}{\partial s}. \quad (17)$$

The system is supplemented with an expression for the normal component of internal stress

$$N = -K_b \frac{\partial^2 \theta}{\partial s^2}, \quad 0 \leq s \leq L, \quad t > 0.$$

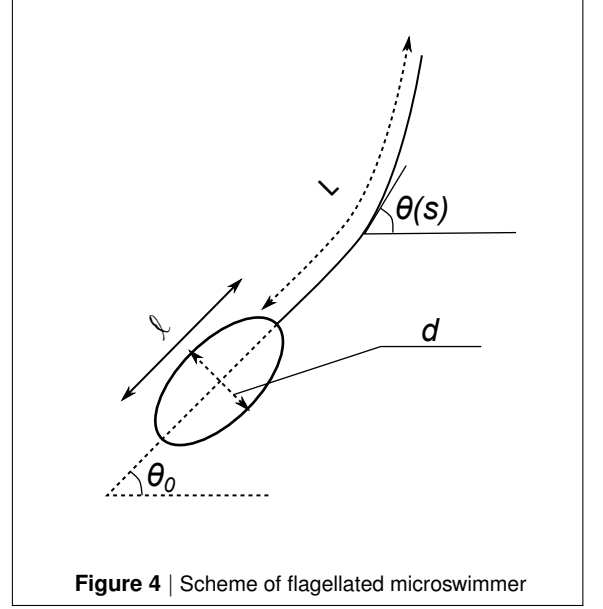


Figure 4 | Scheme of flagellated microswimmer

The system is also endowed with boundary conditions at $s = 0$ (interface body/flagellum):

$$\theta|_{s=0} = \theta_0, \quad (18)$$

$$\frac{1}{\zeta_b} \Lambda|_{s=0} = \frac{\alpha \ell}{4} \sin(2\theta_0) + \frac{1}{\zeta_f} \left[\frac{\partial \Lambda}{\partial s} \Big|_{s=0} + F_p + K_b \frac{\partial \theta}{\partial s} \Big|_{s=0} \frac{\partial^2 \theta}{\partial s^2} \Big|_{s=0} \right], \quad (19)$$

$$- \left(\frac{1}{\alpha \zeta_b} + \frac{\ell^2}{4 \zeta_r} \right) K_b \frac{\partial^2 \theta}{\partial s^2} \Big|_{s=0} = \frac{\beta \gamma \ell}{2} \cos(2\theta_0) + \frac{1}{\alpha \zeta_f} \left[-K_b \frac{\partial^3 \theta}{\partial s^3} \Big|_{s=0} + \frac{\partial \theta}{\partial s} \Lambda \Big|_{s=0} \right], \quad (20)$$

and at $s = L$ (free end of the flagellum):

$$\frac{\partial \theta}{\partial s} \Big|_{s=L} = \frac{\partial^2 \theta}{\partial s^2} \Big|_{s=L} = \Lambda \Big|_{s=L} = 0. \quad (21)$$

Remark: We explain now all the drag coefficients appearing in the system above: ζ_b , ζ_f , ζ_r , and α . To drag the ellipsoidal body with the given velocity V and angular velocity ω one needs to exert the force $\zeta_b V$ and the torque $\zeta_r \omega$, respectively. It can be shown for ellipsoids that the drag coefficients ζ_b and ζ_r are related through the following expression:

$$\zeta_r = \frac{\ell^2}{6} \zeta_b. \quad (22)$$

To drag an infinitesimal (small) piece of the flagellum of length Δs with velocity $V_\tau \boldsymbol{\tau} + V_n \mathbf{n}$ one needs to exert the drag force $\zeta_f \Delta s (\alpha V_\tau \boldsymbol{\tau} + V_n \mathbf{n})$. As it was mentioned above, the parameter α takes into account that drag coefficients in normal and tangent directions are different for the flagellum.

B Results of Two Scale Asymptotic Expansions

Original PDE system non-dimensionalized After the non-dimensionalization

$$\tilde{s} = \frac{s}{L}, \quad \tilde{t} = \gamma t, \quad \tilde{\Lambda} = \frac{\Lambda}{\zeta_f \gamma L^2}$$

we obtain the following PDE system of MMFS with $t > 0$ and $0 < s < 1$:

$$\begin{cases} \frac{d\theta_0}{dt} = -((1 - \beta) \sin^2 \theta_0 + \beta \cos^2 \theta_0) + \frac{3k_r}{r} N_0, & (23) \\ \frac{\partial \theta}{\partial t} = -\frac{1}{\varepsilon \alpha} \frac{\partial^4 \theta}{\partial s^4} + \left(\frac{1}{\alpha} \Lambda + \frac{1}{\varepsilon} \left(\frac{\partial \theta}{\partial s} \right)^2 \right) \frac{\partial^2 \theta}{\partial s^2} + \left(\frac{\alpha + 1}{\alpha} \frac{\partial \Lambda}{\partial s} + f_p \right) \frac{\partial \theta}{\partial s} - \sin^2(\theta), & (24) \\ \frac{\partial^2 \Lambda}{\partial s^2} = \frac{1}{\alpha} \left(\frac{\partial \theta}{\partial s} \right)^2 \Lambda - \frac{1}{\varepsilon} \left(\frac{\partial^2 \theta}{\partial s^2} \right)^2 - \frac{1}{2} \sin(2\theta) - \frac{(\alpha + 1)}{\alpha \varepsilon} \frac{\partial^3 \theta}{\partial s^3} \frac{\partial \theta}{\partial s}, & (25) \end{cases}$$

where we dropped tildes in notations for s , t , and Λ , as well as introduce the additional parameters:

$$\varepsilon = \frac{\zeta_f \gamma L^4}{K_b}, \quad f_p = \frac{F_p}{\zeta_f \gamma L}, \quad k_r = \frac{L \zeta_f}{\zeta_b}, \quad r = \frac{\ell}{L}.$$

In what follows, we obtain asymptotic formulas in the limit $\varepsilon \rightarrow 0$.

Equations at $s = 0$:

$$\begin{cases} N_0 = -\frac{1}{\varepsilon} \frac{\partial^2 \theta}{\partial s^2} \Big|_{s=0}, \quad \theta|_{s=0} = \theta_0, & (26) \end{cases}$$

$$\begin{cases} k_r \Lambda|_{s=0} = \frac{\alpha r}{4} \sin(2\theta_0) + \frac{\partial \Lambda}{\partial s} \Big|_{s=0} + f_p - \frac{\partial \theta}{\partial s} \Big|_{s=0} N_0, & (27) \end{cases}$$

$$\begin{cases} \sigma k_r N_0 = \beta \frac{\alpha r}{2} \cos(2\theta_0) - \frac{1}{\varepsilon} \frac{\partial^3 \theta}{\partial s^3} \Big|_{s=0} + \frac{\partial \theta}{\partial s} \Big|_{s=0} \Lambda|_{s=0}. & (28) \end{cases}$$

Here $\sigma = 1 + \frac{3\alpha}{2}$.

Equations at $s = 1$:

$$\frac{\partial \theta}{\partial s} \Big|_{s=1} = \frac{\partial^2 \theta}{\partial s^2} \Big|_{s=1} = \Lambda \Big|_{s=1} = 0. \quad (29)$$

Multiscale expansion

$$\begin{cases} \theta(s, t, \tau) = \theta^0(s, t, \tau) + \varepsilon \theta^1(s, t, \tau) + \dots, \\ \theta_0(t, \tau) = \theta_0^0(t, \tau) + \varepsilon \theta_0^1(t, \tau) + \dots, \\ \Lambda(s, t, \tau) = \Lambda^0(s, t, \tau) + \varepsilon \Lambda^1(s, t, \tau) + \dots, \\ N_0(t, \tau) = N_0^0(t, \tau) + \varepsilon N_0^1(t, \tau) + \dots, \end{cases}$$

Here $\tau = \varepsilon t$ (slow time).

Modified Jeffery Equation for θ_0^0 The equation for θ_0^0 is obtained by collecting all terms at level ε^0 in (23):

$$\frac{\partial \theta_0^0}{\partial t} = - \left((1 - \beta) \sin^2 \theta_0^0 + \beta \cos^2 \theta_0^0 \right) + \frac{3k_r}{r} N_0^0 \quad (30)$$

This is not a closed equation for θ_0^0 because of the unknown term $\frac{3k_r}{r} N_0^0$ in the equation (30). In order to find this term (in terms of θ_0^0) first note that due to the first equation in (26) we have

$$N_0^0 = - \frac{\partial^2 \theta^1}{\partial s^2} \Big|_{s=0}. \quad (31)$$

Next, expanding equation (24) and collecting all terms at ε^{-1} we get

$$0 = - \frac{1}{\alpha} \frac{\partial^4 \theta^0}{\partial s^4} + \left(\frac{\partial \theta^0}{\partial s} \right)^2 \frac{\partial^2 \theta^0}{\partial s^2}, \quad 0 < s < 1, \quad (32)$$

To write boundary conditions θ^0 at $s = 0$ collect terms at ε^{-1} in the first equation in (26) and (28):

$$\frac{\partial^2 \theta^0}{\partial s^2} \Big|_{s=0} = \frac{\partial^3 \theta^0}{\partial s^3} \Big|_{s=0} = 0. \quad (33)$$

Equations in (29) give boundary conditions for θ^0 at $s = 1$:

$$\frac{\partial \theta^0}{\partial s} \Big|_{s=1} = \frac{\partial^2 \theta^0}{\partial s^2} \Big|_{s=1} = 0. \quad (34)$$

Thus, θ^0 does not depend on s and $\theta^0(s, t, \tau) = \theta_0^0(t, \tau)$:

$$\frac{\partial^i \theta^0}{\partial s^i} \equiv 0, \quad i = 1, 2, 3, \dots \quad (35)$$

Due to (35), the equation for θ^1 which is obtained by collecting all terms at ε^0 in can be written as

$$\frac{\partial^4 \theta^1}{\partial s^4} = - \underbrace{\alpha \left(\frac{\partial \theta_0^0}{\partial t} + \sin^2 \theta_0^0 \right)}_{=: \chi} \quad (36)$$

Thus, taking into account (29) we obtain

$$\frac{\partial^3 \theta^1}{\partial s^3} = \chi \cdot (s - 1) + C_1, \quad (37)$$

$$\frac{\partial^2 \theta^1}{\partial s^2} = \frac{1}{2} \chi \cdot (s - 1)^2 + C_1 \cdot (s - 1), \quad (38)$$

Here C_1 may depend on t and τ , but not on s . In order to find C_1 , use (31), (35) to substitute (37) and (38) with $s = 0$ into (28) at level ε^0 :

$$C_1 = \frac{\sigma k_r + 2}{2(\sigma k_r + 1)} \chi + \frac{\beta \alpha r}{2(\sigma k_r + 1)} \cos(2\theta_0^0). \quad (39)$$

Now we are in position to find the unknown term in the equation (30):

$$\begin{aligned} \frac{3k_r}{r} N_0^0 &= - \frac{3k_r}{r} \frac{\partial^2 \theta^1}{\partial s^2} \Big|_{s=0} = \frac{3k_r}{2r} (-\chi + 2C_1) \\ &= \frac{3k_r}{2r(\sigma k_r + 1)} (\chi + \beta \alpha r \cos(2\theta_0^0)) \\ &= - \frac{3\alpha k_r}{2r(\sigma k_r + 1)} \left\{ \frac{\partial \theta_0^0}{\partial t} + \sin^2 \theta_0^0 \right\} + \frac{3\beta \alpha k_r}{2(\sigma k_r + 1)} \cos 2\theta_0^0. \end{aligned} \quad (40)$$

In order substitute (40) into (30) we note that due to a simple trigonometric identity

$$- \sin^2 \theta_0^0 - B \cos(2\theta_0^0) = -(1 - B) \sin^2 \theta_0^0 - B \cos^2 \theta_0^0, \quad (41)$$

with $B = \beta$, the equation (30) can be written as follows:

$$\frac{\partial \theta_0^0}{\partial t} + \sin^2 \theta_0^0 = -\beta \cos 2\theta_0^0 + \frac{3k_r}{r} N_0^0. \quad (42)$$

Use (40) to write (42) in the form

$$\left[1 + \frac{3\alpha k_r}{2r(\sigma k_r + 1)} \right] \left\{ \frac{\partial \theta_0^0}{\partial t} + \sin^2 \theta_0^0 \right\} = -\beta \left[1 - \frac{3\alpha k_r}{2(\sigma k_r + 1)} \right] \cos(2\theta_0^0),$$

or if one divides by $1 + 3\alpha k_r / (2r(\sigma k_r + 1))$ and uses identity (41) for

$$B = b := \beta r \frac{2\sigma k_r + 2 - 3\alpha k_r}{2r\sigma k_r + 2r + 3\alpha k_r}, \quad (43)$$

then

$$\frac{\partial \theta_0^0}{\partial t} + \sin^2(\theta_0^0) = -b \cos(2\theta_0^0), \quad (44)$$

or, equivalently,

$$\frac{\partial \theta_0^0}{\partial t} = -(1 - b) \sin^2 \theta_0^0 - b \cos^2 \theta_0^0. \quad (45)$$

The equation (45) is of the form of the Jeffery equation, and the main conclusion here is that in the limit of the rigid flagellum $K_b \rightarrow \infty$ (equivalently, $\varepsilon \rightarrow 0$), the swimmer with the body shape parameter β behaves as the ellipse with no flagellum and with the shape parameter b defined in (43) in place of β .

We note that for typical values of parameters σ , k_r , and α , the parameter b introduced in (43) can be computed by

$$b = \frac{r\beta}{1 + 2r}.$$

Asymptotic formula for elastic stress Q In this subsection we find asymptotic formula for elastic stress $Q^0(t, \tau, s)$, whose the normal and tangential components are N^0 and Λ^0 , respectively. The super-index 0 means that we search for values as $\varepsilon \rightarrow 0$.

To find N^0 we first note that the equality (31) holds for all $0 \leq s \leq 1$ (not only for $s = 0$ as in (31)):

$$N^0 = -\frac{\partial^2 \theta^1}{\partial s^2}, \quad 0 \leq s \leq 1. \quad (46)$$

From (36), (39) and (44) we can easily get

$$\chi = \alpha b \cos(2\theta_0) \quad \text{and} \quad C_1 = \sigma_1 \cos(2\theta_0^0), \quad (47)$$

where

$$\sigma_1 := \frac{\alpha b(\sigma k_r + 2) + \alpha \beta r}{2(\sigma k_r + 1)} \quad (48)$$

Thus, from (38), (46) and (47) it follows that

$$N_0 = -\left(\frac{\alpha b}{2}(s-1)^2 + \sigma_1(s-1)\right) \cos(2\theta_0^0). \quad (49)$$

In order to find Λ^0 , we collect all terms at level ε^0 in the equation (25) using (35):

$$\frac{\partial^2 \Lambda^0}{\partial s^2} = -\frac{1}{2} \sin(2\theta_0^0). \quad (50)$$

In view of (29) (a boundary condition at $s = 1$) and that θ_0^0 is independent from s we have

$$\Lambda^0 = -\frac{1}{4}(s-1)^2 \sin 2\theta_0^0 + C_2(s-1). \quad (51)$$

In order to find C_2 use (27):

$$-\frac{k_r}{4} \sin 2\theta_0^0 - k_r C_2 = \frac{\alpha r}{4} \sin 2\theta_0^0 + \frac{1}{2} \sin 2\theta_0^0 + C_2 + f_p. \quad (52)$$

Thus,

$$C_2 = -\sigma_2 \sin 2\theta_0^0 - \frac{F_p}{1 + k_r}, \quad \text{where} \quad \sigma_2 := \frac{k_r + \alpha r + 2}{4(1 + k_r)}. \quad (53)$$

In particular,

$$\Lambda^0 = \left(-\frac{1}{4}(s-1)^2 - \sigma_2(s-1)\right) \sin 2\theta_0^0 - \frac{f_p}{1 + k_r}(s-1). \quad (54)$$

Asymptotic formulas for N^0 and Λ^0 in the original scaling:

$$N^0 = -\zeta_f \gamma \left(\frac{\alpha b}{2}(s-L)^2 + L\sigma_1(s-L)\right) \cos 2\theta_0^0. \quad (55)$$

$$\Lambda^0 = -\zeta_f \gamma \left(\frac{1}{4}(s-L)^2 + L\sigma_2(s-L)\right) \sin 2\theta_0^0 - \frac{f_p}{1 + k_r}(s-L). \quad (56)$$

Contribution to effective viscosity *The elastic contribution.* From the Kirkwood formula (see Eqn. (2) in the paper) using integration by parts we obtain

$$\eta_{\text{elastic}} = \frac{\Phi}{2\dot{\gamma}\eta_0} \langle \int_0^L (Q \cdot \mathbf{e}_2) (\boldsymbol{\tau} \cdot \mathbf{e}_1) + (Q \cdot \mathbf{e}_1) (\boldsymbol{\tau} \cdot \mathbf{e}_2) ds \rangle_{\theta_0} \quad (57)$$

where $\mathbf{e}_1 = (1, 0)$, $\mathbf{e}_2 = (0, 1)$, and $\langle \cdot \rangle_{\theta_0}$ denotes the expected value with respect to probability distribution function $P(\theta_0)$ of body orientation angles (see Results section where $P(\theta_0)$ was introduced):

$$\langle g \rangle_{\theta_0} := \frac{q}{2\pi} \int_0^{2\pi} \frac{g(\theta_0)}{1 - (1 - 2b) \cos(2\theta_0)} d\theta_0, \quad (58)$$

where $q = \sqrt{1 - (1 - 2b)^2}$.

We search for the leading term in ε which is of the order 1. Thus, assume $\boldsymbol{\tau} = (\cos \theta, \sin \theta) \approx (\cos \theta_0, \sin \theta_0)$. Then after some straightforward calculations we obtain

$$\eta_{\text{elastic}} = \frac{\Phi}{\dot{\gamma}\eta_0} \langle \int_0^L \Lambda^0(s; \theta_0) \sin 2\theta_0 + N^0(s; \theta_0) \cos(2\theta_0) ds \rangle_{\theta_0} \quad (59)$$

Substituting (56) and (55) (with θ_0 instead of θ_0^0) into (59) we get

$$\eta_{\text{elastic}} = \Phi \frac{L^3}{\eta_0} Z_{\text{elastic}}(\beta, r), \quad (60)$$

where

$$\begin{aligned} Z_{\text{elastic}}(\beta, r) = \zeta_f \frac{r\beta}{12(1 + 2r - 2r\beta)} \left\{ (2r + 5) \sqrt{1 + 2r - r\beta} \left(2r + 1 - 2\sqrt{r\beta} \sqrt{1 + 2r - \beta r} \right) \right. \\ \left. + 3\sqrt{r\beta}(3r + 2)(2r + 1 - 2\sqrt{r\beta}) \right\}. \end{aligned} \quad (61)$$

The propulsion contribution. The Kirkwood formula for propulsive contribution has the form

$$\begin{aligned} \eta_{\text{propulsion}} &= \frac{\Phi}{2\dot{\gamma}\eta_0} \langle -F_p \int_0^L (\boldsymbol{\tau} \cdot \mathbf{e}_1) (y(s) - y(0)) + (\boldsymbol{\tau} \cdot \mathbf{e}_2) (x(s) - x(0)) ds \rangle_{\theta_0} \\ &= -\frac{F_p \Phi}{2\dot{\gamma}\eta_0} \langle \int_0^L \int_0^s \cos \theta(s) \sin \theta(w) + \sin \theta(s) \cos \theta(w) dw ds \rangle_{\theta_0} \end{aligned} \quad (62)$$

Substituting expansion $\theta = \theta^0 + \varepsilon\theta^1 + \dots$ into (62) after some cumbersome calculations we obtain

$$\eta_{\text{propulsion}} = -\frac{F_p \Phi}{2\dot{\gamma}\eta_0} \langle \frac{L^2}{2} \sin(2\theta_0) + \varepsilon L \cos(2\theta_0) \int_0^L \theta^1(s) ds \rangle_{\theta_0} + o(\varepsilon). \quad (63)$$

The first term has zero contribution after averaging with respect to θ_0 , and the equality (63) becomes

$$\eta_{\text{propulsion}} = -\varepsilon \frac{\Phi F_p L^2}{\eta_0 \dot{\gamma}} Z_{\text{prop}}(\beta, r), \quad (64)$$

where

$$Z_{\text{prop}}(\beta, r) = \beta \frac{r(17 + 10r)(2r + 1 - q\sqrt{2r + 1})}{120(2r + 1 - \beta r)^2}. \quad (65)$$

References

1. Wu, X.-L. & Libchaber, A. Particle Diffusion in a Quasi-Two-Dimensional Bacterial Bath. *Physical Review Letters* **84**, 3017–3020 (2000).
2. Dombrowski, C., Cisneros, L., Chatkaew, S., Goldstein, R. E. & Kessler, J. O. Self-concentration and large-scale coherence in bacterial dynamics. *Physical Review Letters* **93**, 098103 (2004).
3. Sokolov, A., Aranson, I., Kessler, J. & Goldstein, R. Concentration dependence of the collective dynamics of swimming bacteria. *Physical Review Letters* **98**, 158102 (2007).
4. Drecher, K., Dunkel, J., Cisneros, L., Ganguly, S. & Goldstein, R. Fluid dynamics and noise in bacterial cell-cell and cell-surface scattering. *Proceedings of the National Academy of Sciences* **108**, 10940–10945 (2011).
5. Rusconi, R., Guasto, J. S. & Stocker, R. Bacterial transport suppressed by fluid shear. *Nature physics* **10**, 212–217 (2014).
6. Stocker, R. Marine microbes see a sea of gradients. *Science* **338**, 628–633 (2012).
7. Wensink, H. H. *et al.* Meso-scale turbulence in living fluids. *Proceedings of the National Academy of Sciences* **109**, 14308–14313 (2012).
8. Sokolov, A. & Aranson, I. Physical properties of collective motion in suspensions of bacteria. *Physical Review Letters* **109**, 248109 (2012).
9. Sokolov, A. & Aranson, I. Reduction of viscosity in suspension of swimming bacteria. *Physical Review Letters* **103**, 148101 (2009).
10. Gachelin, J. *et al.* Non-Newtonian Viscosity of Escherichia coli Suspensions. *Physical Review Letters* **110**, 268103 (2013).
11. López, H., Gachelin, J., Douarche, C., Auradou, H. & Clément, E. Turning bacteria suspensions into superfluids. *Physical Review Letters* **115**, 028301 (2015).
12. Sokolov, A., Apodaca, M., Grzybowski, B. & Aranson, I. Swimming bacteria power microscopic gears. *Proceedings of the National Academy of Sciences of the United States of America* **107**, 969–974 (2009).
13. Di Leonardo, R. *et al.* Bacterial ratchet motors. *Proceedings of the National Academy of Sciences* **107**, 9541–9545 (2010).
14. Kaiser, A. *et al.* Transport powered by bacterial turbulence. *Physical review letters* **112**, 158101 (2014).
15. Sokolov, A., Goldstein, R., Feldchtein, F. & Aranson, I. Enhanced mixing and spatial instability in concentrated bacterial suspensions. *Physical Review E* **80**, 031903 (2009).
16. Pushkin, D. O. & Yeomans, J. M. Stirring by swimmers in confined microenvironments. *Journal of Statistical Mechanics: Theory and Experiment* **2014**, P04030 (2014).
17. Ariel, G. *et al.* Swarming bacteria migrate by lévy walk. *Nature communications* **6** (2015).

18. Marcos, Fu, H. C., Powers, T. R., Stocker, R. *et al.* Bacterial rheotaxis. *Proceedings of the National Academy of Sciences* **109**, 4780–4785 (2012).
19. Sokolov, A. & Aranson, I. S. Rapid expulsion of microswimmers by a vortical flow. *Nature Communications* **7**, 1114 (2016).
20. Son, K., Guasto, J. & Stocker, R. Bacteria can exploit a flagellar buckling instability to change direction. *Nature Physics* **9**, 494–498 (2013).
21. Vogel, R. & Stark, H. Motor-driven bacterial flagella and buckling instabilities. *European Physical Journal E: Soft Matter* **35**, 1–15 (2012).
22. Vogel, R. & Stark, H. Rotation-induced polymorphic transitions in bacterial flagella. *Physical Review Letters* **110**, 158104 (2013).
23. Brumley, D., Rusconi, R., Son, K. & Stocker, R. Flagella, flexibility and flow: Physical processes in microbial ecology. *The European Physical Journal: Special Topics* **224**, 3119–3140 (2015).
24. Zöttl, A. & Stark, H. Nonlinear dynamics of a microswimmer in poiseuille flow. *Physical Review Letters* **108**, 218104 (2012).
25. Zöttl, A. & Stark, H. Periodic and quasiperiodic motion of an elongated microswimmer in Poiseuille flow. *The European Physical Journal E* **36**, 1–10 (2013).
26. Adhyapak, T. C. & Stark, H. Zipping and entanglement in flagellar bundle of *E. coli*: Role of motile cell body. *Phys. Rev. E* **92**, 052701 (2015).
27. Tournus, M., Kirshtein, A., Berlyand, L. & Aranson, I. Flexibility of bacterial flagella in external shear results in complex swimming trajectories. *Journal of the Royal Society Interface* **12**, 20140904 (2015).
28. Haines, B., Aranson, I., Berlyand, L. & Karpeev, D. Effective viscosity of dilute bacterial suspensions: a two-dimensional model. *Physical Biology* **5**, 046003 (2008).
29. Haines, B., Sokolov, A., Aranson, I., Berlyand, L. & Karpeev, D. Three-dimensional model for the effective viscosity of bacterial suspensions. *Physical Review E* **80**, 041922 (2009).
30. Saintillan, D. Extensional rheology of active suspensions. *Physical Review E* **81**, 056307 (2010).
31. Berke, A., Turner, L., Berg, H. & Lauga, E. Hydrodynamic attraction of swimming microorganisms by surfaces. *Physical Review Letters* **101**, 038102 (2008).
32. Rothschild, L. Non-random distribution of bull spermatozoa in a drop of sperm suspension. *Nature* **198**, 1221 (1963).
33. Berg, H. & Turner, L. Chemotaxis of bacteria in glass capillary arrays. *Escherichia coli*, motility, microchannel plate, and light scattering. *Biophysical Journal* **58**, 919–930 (1990).
34. DiLuzio, W. R. *et al.* *Escherichia coli* swim on the right-hand side. *Nature* **435**, 1271–1274 (2005).
35. Ramia, M., Tullock, D. & Phan-Thien, N. The role of hydrodynamic interaction in the locomotion of microorganisms. *Biophysical Journal* **65**, 755–778 (1993).
36. Frymier, P., Ford, R., Berg, H. & Cummings, P. Three-dimensional tracking of motile bacteria near a solid planar surface. *Proceedings of the National Academy of Sciences: Biophysics* **92**, 6195–6199 (1995).
37. Vigeant, M., Ford, R., Wagner, M. & Tamm, L. Reversible and Irreversible Adhesion of Motile *Escherichia coli* Cells Analyzed by Total Internal Reflection Aqueous Fluorescence Microscopy. *Applied and Environmental Microbiology* **68**, 2794–2801 (2002).
38. Mushenheim, P. *et al.* Effects of confinement, surface-induced orientations and strain on dynamical behaviors of bacteria in thin liquid crystalline films. *Soft Matter* **11**, 6821–6831 (2015).
39. Zhou, S., Sokolov, A., Lavrentovich, O. D. & Aranson, I. S. Living liquid crystals. *Proceedings of the National Academy of Sciences* **111**, 1265–1270 (2014).
40. Zhou, S., Sokolov, A., Aranson, I. & Lavrentovich, O. Control of dynamic behavior of bacteria by lyotropic chromonic liquid crystals with homeotropic orientation of director. *in preparation*.
41. Batchelor, G. *An Introduction to Fluid Dynamics* (Cambridge University Press, Cambridge, 1967).
42. Kim, S. & Karrila, J. *Microhydrodynamics: Principles and Selected Applications* (Dover, 1991).
43. Ryan, S., Haines, B., Berlyand, L., Ziebert, F. & Aranson, I. Viscosity of bacterial suspensions: Hydrodynamic interactions and self-induced noise. *Physical Review E* **83**, 050904 (2011).
44. Batchelor, G. The stress system in a suspension of force-free particles. *Journal of Fluid Mechanics* **41**, 545–570 (1970).
45. Fürthauer, S., Stempel, M., Grill, S. & Jülicher, F. Active chiral fluids. *The European Physical Journal E, Soft matter* **35**, 89 (2012).
46. Kirkwood, J. & Auer, P. The Visco-Elastic Properties of Solutions of Rod-Like Macromolecules. *The Journal of Chemical Physics* **19**, 281–283 (1951).
47. Doi, M. & Edwards, S. *The Theory of Polymer Dynamics* (Oxford University Press, 1988).
48. Ziebert, F. & Aranson, I. Rheological and structural properties of dilute active filament solutions. *Physical Review E* **77**, 011918 (2008).
49. Einstein, A. Eine neue bestimmung der moleküldimensionen. *Annalen der Physik* **324**, 289–206 (1906).
50. Jeffery, G. The Motion of Ellipsoidal Particles Immersed in a Viscous Fluid. *Proceedings of the Royal Society A* **102**, 161–179 (1922).
51. Darnton, N. & Berg, H. Force-extension measurements on bacterial flagella: triggering polymorphic transformations. *Biophysical journal* **92**, 2230–2236 (2007).
52. Greenberg, E. & Canale-Parola, E. Motility of flagellated bacteria in viscous environments. *Journal of bacteriology* **132**, 356–358 (1977).
53. Schneider, W. & Doetsch, R. Effect of viscosity on bacterial motility. *Journal of bacteriology* **117**, 696–701 (1974).
54. Keller, J. Effect of viscosity on swimming velocity of bacteria. *Proceedings of the National Academy of Sciences* **71**, 3253–3254 (1974).
55. Alouges, F., DeSimone, A. & Lefebvre, A. *Biological fluid dynamics, nonlinear partial differential equations // Encyclopedia of Complexity and Systems Science*. (2009).
56. Marcos. *Bacteria in shear flow*. Ph.D. thesis (2011).
57. Berg, H. & Anderson, R. Bacteria swim by rotating their flagellar filaments. *Nature* **245**, 380–382 (1973).
58. Roper, M. *et al.* On the dynamics of magnetically driven elastic filaments. *Journal of Fluid Mechanics* **554**, 167–190 (2006).